

Microneedle Array Electrodes Fabricated With 3D Printing Technology for High-Quality Electrophysiological Acquisition

Jianyu Fu^{ID}, Shanyong Huang, Jianglang Cao, Jianping Huang, Debin Xu, Naifu Jiang^{ID}, *Member, IEEE*, Xiangxin Li^{ID}, Guanglin Li^{ID}, *Senior Member, IEEE*, and Peng Fang^{ID}, *Senior Member, IEEE*

Abstract—Electrophysiological recordings are vital in assessing biological functions, diagnosing diseases, and facilitating biofeedback and rehabilitation. The applications of conventional wet (gel) electrodes often come with some limitations. Microneedle array electrodes (MAEs) present a possible solution for high-quality electrophysiological acquisition, while the prior technologies for MAE fabrication have been either complex, expensive, or incapable of producing microneedles with uniform dimensions. This work employed a projection stereolithography (P μ SL) 3D printing technology to fabricate MAEs with micrometer-level precision. The MAEs were compared with gel and flat electrodes on electrode-skin interface impedance (EII) and performances of EMG and ECG acquisition. The experimental results indicate that the P μ SL 3D printing technology contributed to an easy-to-perform and low-cost fabrication approach for MAEs. The developed MAEs exhibited promising EII and enabled a stable EMG and ECG acquisition in different conditions without inducing skin allergies, inflammation, or injuries. This research lies in the development of a type of customizable MAE with considerable biomedical application potentials for ultra-minimally invasive or non-invasive electrophysiological acquisition.

Index Terms—Microneedle array electrode, electrophysiological signal, EMG, ECG, 3D printing.

I. INTRODUCTION

ELECTROPHYSIOLOGICAL signals play a significant role in assessing biological functions, diagnosing diseases, and facilitating biofeedback and rehabilitation. By monitoring and analyzing electrophysiological signals, a comprehensive understanding of pathological and physiological states of human bodies can be achieved [1], [2]. Especially in clinical practice, the fast progress of electrophysiology has facilitated the widespread applications of electromyography (EMG), electrocardiography (ECG), and electroencephalography (EEG). For instance, the contraction, relaxation, and coordination abilities of muscles can be evaluated through EMG signals, facilitating the identification of anomalies such as muscle weakness, spasms, or tremors [3], [4]; a continuous recording of ECG signals enables the detection of abnormalities in cardiac electrical conduction and rhythm, the assessment of cardiac muscle contraction and relaxation, and the assist in diagnosing cardiac pathologies, arrhythmias, and myocardial ischemia [5], [6]; analysis of EEG signals allows for the identification of abnormal patterns in brain electrical activity such as epileptic seizures or anomalous changes in sleep stage electroencephalograms, aiding in the diagnosis of epilepsy and sleep disorders [7], [8]. Meanwhile, due to the development of biopotential electrodes and signal processing algorithms, the utilization of non-invasive methods for acquiring electrophysiological signal has gained prominence in human-machine interface studies [9].

Biopotential electrodes serve the purpose of converting ionic current within human bodies into an electronic current that can be effectively utilized by external electronic systems [10]. Conventional biopotential electrodes, known as wet electrodes or gel electrodes, are typically constructed using a combination of silver, silver chloride (Ag/AgCl), and conductive gel. As the most typical electrodes used in clinical practice, they offer the advantage of non-invasively capturing high-resolution electrophysiological signals. However, the disadvantages of wet electrodes significantly limit their further application. The pre-treatment of electrodes before use

Manuscript received 9 November 2023; revised 3 June 2024; accepted 8 June 2024. Date of publication 3 July 2024; date of current version 12 July 2024. This work was supported in part by the National Natural Science Foundation of China under Grant U21A20479 and Grant 81927804, in part by the Chinese Academy of Sciences (CAS) Youth Innovation Promotion Association under Grant Y2022094, in part by the Science and Technology Program of Guangdong Province under Grant 2022A0505090007, in part by Shenzhen Fundamental Research Program under Grant JCYJ20200109114805984 and Grant JCYJ20210324101601005, and in part by Shenzhen Engineering Laboratory of Neural Rehabilitation Technology. (*Corresponding author: Peng Fang.*)

This work involved human subjects or animals in its research. Approval of all ethical and experimental procedures and protocols was granted by the Institutional Review Board of Shenzhen Institute of Advanced Technology, Chinese Academy of Sciences, under IRB Number: SIAT-IRB-190315-H0325.

Jianyu Fu and Shanyong Huang are with the Southern University of Science and Technology, Shenzhen 518055, China, and also with Shenzhen Institute of Advanced Technology, Chinese Academy of Sciences, Shenzhen 518055, China.

Jianglang Cao is with Shenzhen Institute of Advanced Technology, Chinese Academy of Sciences, Shenzhen 518055, China.

Jianping Huang, Debin Xu, Naifu Jiang, Xiangxin Li, Guanglin Li, and Peng Fang are with Shenzhen Institute of Advanced Technology, Chinese Academy of Sciences, Shenzhen 518055, China, and also with the University of Chinese Academy of Sciences, Beijing 100049, China (e-mail: lixx@siat.ac.cn; gl.li@siat.ac.cn; peng.fang@siat.ac.cn).

Digital Object Identifier 10.1109/TNSRE.2024.3422489

involves time-consuming procedures such as hair removal, skin abrasion, and application of conductive gel. Besides, while wet electrodes utilize conductive gel to maintain optimal skin conductivity, extended exposure to this gel can lead to discomfort or allergic reactions, especially in individuals with sensitive skins like infants and the elderly. In addition, the conductive gel is sensitive to humidity and temperature of surrounding environment, which would limit their application scenarios [11], [12], [13]. In dry conditions, the conductive gel can dry out more quickly, resulting in decreased contact between electrode and skin, thereby affecting the quality of signals. In order to overcome the above challenges, researchers have proposed dry electrodes as an alternative option [14]. Commonly used dry electrodes are typically flat electrodes, which operate without a demand for conductive gel, making them more suitable for long-term electrophysiological acquisition. However, in comparison to wet electrodes, dry electrodes usually exhibit higher electrode-skin interface impedance (EII) [15], [16]. Moreover, the interface between dry electrodes and skin is less stable and more susceptible to interference from body motions [17], [18]. In recent years, within the field of brain-computer interfaces, researchers have successfully developed semi-dry electrodes that require only a minimal amount of electrolyte solution to overcome the respective drawbacks of wet and dry electrodes. Semi-dry electrodes can not only collect reliable EEG signals comparable to those with wet electrodes, but also offer a quick and convenient use associated with dry electrodes. However, the long-term use of semi-dry electrodes is still constrained by the dependence on electrolyte solution [19], [20], [21].

Generally, electrodes are employed on skin surface to capture electrophysiological signals. The skin, being the largest organ of human body, comprises several layers including the epidermis, dermis, and subcutaneous tissue. The epidermis, the outermost layer of the skin, has an approximate thickness of 220 μm and is composed of the stratum corneum and the viable epidermis [22]. The stratum corneum plays a crucial role in shielding the body from mechanical, thermal, chemical, biological, and radiation threats present in the environment, with a thickness of about 10 to 40 μm . It consists of dead cells, leading to high impedance and poor conductivity [23], [24]. Conversely, the viable epidermis beneath the stratum corneum exhibits high conductivity. The dermis below the epidermis, which encompasses blood vessels and pain receptors of nerves, with thickness ranges from approximately 0.6 to 3 mm [22]. Based on the structure and properties of skin, if an electrode can be designed to penetrate the high-impedance stratum corneum and establish a direct electrical connection between the external circuit and the low-impedance viable epidermis, the challenges encountered by the existing various types of electrodes in applications might be partly overcome. In light of this principle, researchers have proposed a conception of microneedle array electrode (MAE).

MAEs possess a special structure and offer distinct advantages in electrophysiological signal acquisition. To begin with, the prior preparation and application of conductive gel are not required, resulting in shorter preparation time and avoiding adverse reactions such as skin irritation, allergies, and dam-

age [25], [26]. In addition, the microneedles in MAEs are capable of effectively penetrating through the high-impedance stratum corneum, establishing a direct contact with the highly conductive active viable epidermis layer, which significantly reduces the EII. Moreover, the penetration of microneedle to the skin ensures a reliable fixation of electrode, resulting in a more stable skin-electrode interface and reduced interference from motion artifacts [27]. Lastly, the penetration is minimally invasive and does not cause damage to the dermis, thereby avoiding stimulation of dermal nerves [28], [29].

The concept of employing MAEs for electrophysiological acquisition was initially introduced in the year of 2000 [11]. Currently, various techniques have been utilized for MAE fabrication. Hsu et al. utilized photolithography with etching to fabricate MAEs with micro-hook-shaped structures on silicon wafers [30], while Fofonoff et al. employed electrical discharge machining to fabricate MAEs based on titanium rods [31]. But these techniques entail complex procedures as well as expensive instrumentation and super clean room, rendering them not much practical for large-scale manufacturing. Chen et al. and Pan et al. attempted to achieve a simple and rapid fabrication of MAEs using a magnetization-induced self-assembly method [32], [33]. Ren et al. utilized the magnetorheological drawing lithography to prepare MAEs on flexible printed circuit boards and polyethylene-terephthalate films [34]. However, this way relies on manual manipulation and cannot yield microneedles with uniform dimensions. The magnetorheological drawing lithography employs curable magnetorheological fluids for MAE preparation, while further investigation is required to assess the biocompatibility of curable magnetorheological fluids. Krieger et al. employed 3D printing technology using ultraviolet-curable resin to produce MAEs with uniform structures and customizable features [35]. This 3D printing technology only exhibits high precision in the fabrication of millimeter-scale microneedle, which does not meet the requirements for ultra-minimally invasive electrodes.

In this study, we utilized a 3D printing technology of projection stereolithography to fabricate MAEs with micrometer-level precision from photosensitive resin, which are capable of high-quality electrophysiological acquisition for clinical use. We prepared MAEs with different parameters to investigate the characteristics of EII. In addition, we compared the performances of MAEs, gel electrodes, and flat electrodes in the acquisition of EMG and ECG, where the signal-to-noise ratio (SNR) of EMG signals, the EMG-based classification accuracy (CA) for hand motions, as well as the maximum amplitude and motion artifacts of ECG signals are investigated.

II. MATERIALS AND METHODS

A. Sample Fabrication

To fabricate MAE samples, we employed a 3D printing technique based on Projection Micro Stereolithography (P μ SL). It is a digital light processing-based 3D printing technique which employs regional ultraviolet (UV) projection to instigate localized photo-polymerization, allowing for a high-resolution construction of target electrodes' 3D geometrical shape. The comprehensive procedure for sample fabrication

can be broadly categorized into three stages as shown in Fig. 1. First and foremost, a three-dimensional model of MAE is created by using the computer-aided design (CAD) software. This model is then sliced at a layer thickness of 10 mm, resulting in a series of two-dimensional patterns. In other words, samples are printed layer by layer with a precision of 10 μm per layer. Then, the 2D pattern data are transmitted to the printing system, where a digital micromirror device (DMD) generates a dynamic digital mask and controls the deflection of each micromirror (each pixel on the DMD) based on the image data. As the UV light emitted from the light source reaches the DMD, it is reshaped to match the image data and is projected onto the surface of liquid resin via the final objective lens. This leads to selective exposure and solidification of specific regions, forming the microneedles. In this work, the MAE samples consist of a cubic substrate combined with an array of microneedles in conical shape. The substrate measures 6 mm \times 6 mm \times 0.5 mm, whereas the height of microneedles is $\sim 600 \mu\text{m}$, the diameter of needle tip is $\sim 8 \mu\text{m}$, and the diameter of needle base is $\sim 300 \mu\text{m}$. In this work, we designed samples with three different microneedle densities: 3 \times 3, 6 \times 6, and 9 \times 9 needles on each substrate, corresponding inter-needle center-to-center distances of 2.25, 0.9, and 0.525 mm, respectively. Subsequently, isopropanol is used to dissolve and remove any uncured photosensitive resin and magnetron sputtering technology is employed to coat the non-conductive microneedles first with a 50 nm-thick titanium (Ti) layer and then a 100 nm-thick Aurum (Au) layer to endow the surface of microneedles with good conductivity. Finally, each MAE sample is attached to a metal buckle for electric connection and medical tapes are used to fix the buckles on skin surface for signal acquisition.

In addition, for performance assessment, we prepared flat electrodes with the same parameter as the substrate of MAEs, i.e., 6 mm \times 6 mm \times 0.5 mm, and also included commercially available gel electrodes (*CH3540TD, Cathay, China*) in the follow-up comparative experiments.

B. Equivalent Circuit Models

Fig. 2 depicts the equivalent circuits for the three types of electrodes. When wet electrodes come into contact with skin, as shown in Fig. 2(a), an electrode-gel interface and a gel-epidermis interface are formed. The E_{eq} represents the electrode potential difference in this two-electrode configuration, and E_{sc} is caused by the different ion concentrations at the gel-epidermis interfaces and electrode-gel interfaces. The combination of C_{d} and R_{d} represents the impedance at the electrode-gel interface, while the series R_{es} represents the resistance of the gel. The entire gel-epidermal interface can be modeled as a parallel combination of resistance R_{e} and capacitance C_{e} . The dermis and subcutaneous tissues, primarily composed of blood vessels and nerves, have negligible capacitance, and their impedance can be considered as a pure resistance R_{u} [15], [36].

As reported [36], when wet electrodes are in contact with skin, the gel acts as an electrolyte between the electrode and skin surface, however, in the case of dry electrodes the electrolyte is considered as insufficient. When flat electrodes

contact skin directly, as shown in Fig. 2(b), it is necessary to consider the irregular and unstable contact surface caused by the insufficient electrolytes, as well as the occasional presence of air bubbles between the electrode and skin. Therefore, the resistance R_{es} is replaced by a capacitance C_{es} and a resistance R_{es} in parallel [36].

In the case of microneedles penetrating through the stratum corneum and directly contacting the viable epidermis, as shown in Fig. 2(c), the influence of high-impedance stratum corneum is eliminated, forming a metal-viable epidermis interface. The combination of C_{e} and R_{e} represents the impedance at the metal-viable epidermis interface. R_{u} still represents the pure resistance of the dermis and subcutaneous tissues. Consequently, MAEs theoretically eliminate the influence from the stratum corneum and electrolyte gel, and thereby minimize the impedance at the skin-electrode interface [15], [37].

C. Subjects

In this work, a non-disabled adult male was recruited for EII study; for EMG acquisition, six adult males were recruited, including five non-disabled subjects and a subject with left forearm amputation; for ECG acquisition, the same five non-disabled subjects as for EMG acquisition were tested. The health assessment before experiments indicated that all participants were mentally sound and eligible for the study. The research protocol received endorsement from the Institutional Review Board of Shenzhen Institute of Advanced Technology, Chinese Academy of Sciences (*IRB Number: SIAT-IRB-190315-H0325*). All participants provided written informed consent and authorized the use of photographs for academic and educational purpose.

D. Impedance Characterization

A total of five types of electrodes were compared in the EII measurements: MAEs with 3 \times 3, 6 \times 6, and 9 \times 9 microneedle arrays, gel electrodes, and flat electrodes. The EII was measured by using a two-electrode system with an impedance analyzer (*TH2829C, Tonghui Electronic, China*), with frequency range set from 20 to 2000 Hz. Prior to each measurement, the test area was cleaned with a 75% medical alcohol swab, and then two electrode samples of each type were fixed on the subject's forearm with a center-to-center distance of 3 cm.

Three scenarios were designed for EII measurement as follows, and each scenario was tested at least for three times:

- 1) Static condition: the subject was in a seated position;
- 2) Pressure condition: the subject was in a seated position with the test site subjected to a standard weight of 200 g;
- 3) Dynamic condition: the subject was standing and swinging his test arm continuously.

E. EMG Recording

For EMG recording, three types of electrodes, i.e., MAEs with 9 \times 9 microneedle array, gel electrodes, and flat electrodes, were applied and compared. As shown in Fig. 3(a), two-channel electrodes were placed on a subject's extensor carpi

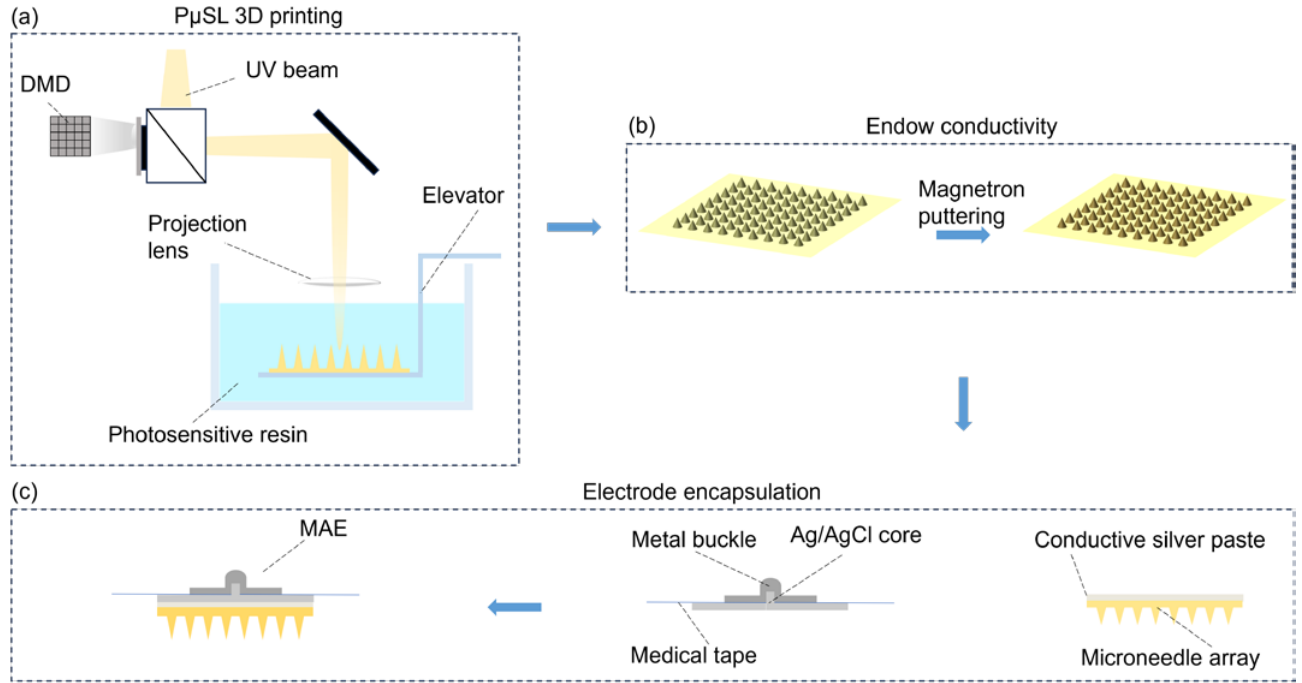


Fig. 1. Schematic diagram of the fabrication procedure for MAEs, where (a) the P μ SL 3D printing technology to prepare MAE models, (b) the magnetron sputtering to deposit conductive layers, and (c) the connection method for MAEs.

radialis longus with a center-to-center distance of 3 cm. An additional two-channel electrodes were placed on the flexor carpi ulnaris. These four-channel electrodes served as the working electrodes, while a reference electrode was attached to the subject's elbow. As indicated in Fig. 3(b), the subject was required to perform a series of six predefined functional hand motions including hand closing (HC), hand opening (HO), wrist extension (WE), wrist flexion (WF), wrist supination (WS), and wrist pronation (WP), in both static (standing still) and dynamic (standing with arm swinging) scenarios. Each motion lasted for 5 s and each series was conducted for three times. To reduce muscle fatigue, there was a 5 s rest between adjacent motions and a 20 s rest before each repetition.

The EMG sampling rate was set to 2000 Hz and signals were processed with *MATLAB*. We implemented a 50 Hz harmonic IIR comb filter and a 400th-order zero phase-shift FIR bandpass filter with a frequency range from 5 to 400 Hz to eliminate possible influences from power line interference and baseline drift, respectively, and then the filtered signals were segmented and combined. Specifically, we extracted the middle 2 s of each 5-second action segment, and these extracted segments were thereafter combined to form the signal segments. Furthermore, we extracted the middle 2 s of the 5-second rest segments between adjacent motions and combined them to form the noise segments.

The SNR of EMG and the EMG-based CA for six functional hand motions were measured to compare the electrode performances. We first calculated the root mean square (RMS) of the signal and noise segments, respectively. The RMS was computed with the following formula:

$$\text{RMS} = \sqrt{\frac{1}{N} \sum_{i=1}^N |X_i|^2}, \quad (1)$$

where N represents the number of samples in the segment, and X_i denotes the individual data values. Then the SNR of signals was computed with the following formula:

$$\text{SNR} = 20 \log_{10} \frac{\text{RMS}_{\text{signal}}}{\text{RMS}_{\text{noise}}}, \quad (2)$$

where $\text{RMS}_{\text{signal}}$ and $\text{RMS}_{\text{noise}}$ represents the RMS of the signal and noise segments, respectively. Besides, we conducted the t -test on the SNR results over the three electrodes.

We utilized a sliding window with a window size of 300 ms and a stride of 150 ms to extract five time-domain features from the time series data, including the Mean, Standard Deviation, Peak, RMS, and Waveform Length. The EMG-based CA of functional motions was computed using a neural network classifier based on the Multi-Layer Perceptron (MLP). The performance of the model was then evaluated using the stratified k -fold cross-validation.

F. ECG Recording

The electrodes used for ECG recording were the same as those used for EMG recording, i.e., MAEs with 9×9 microneedle array, gel electrodes, and flat electrodes. A pair of electrodes of each type was placed on subjects' left chest to acquire ECG signals, and the reference electrode was placed on their left shoulder. Three motion states were designated during signal acquisition, including standing still, walking on a slope, and walking on stairs, with each motion state lasting for 20 s.

The sampling rate for ECG signals was set to 1000 Hz, and the acquired raw data was processed and analyzed with *MATLAB*. We designed a 200th-order zero phase-shift FIR bandpass filter with a frequency range from 1 to 30 Hz to address baseline drift and retain signals within the desired frequency band.

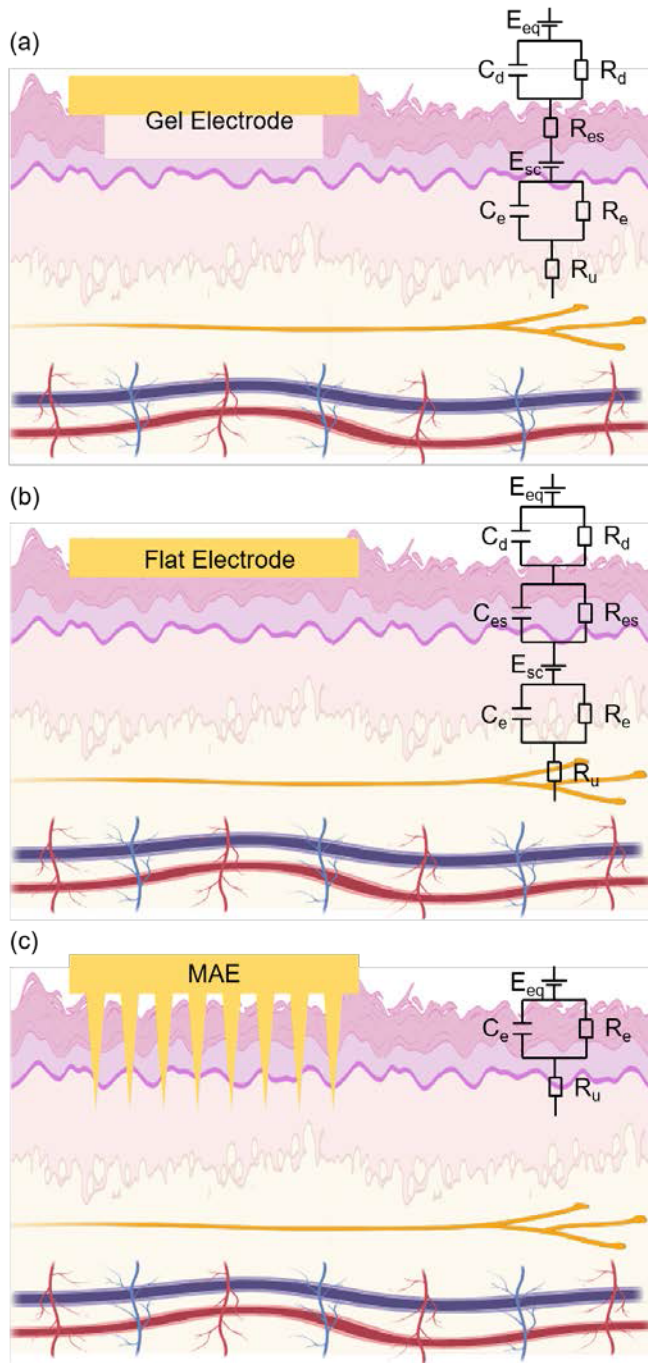


Fig. 2. The equivalent circuits for (a) gel electrode, (b) flat electrode, and (c) MAE.

Three evaluation criteria were employed for electrode performance assessment. First, the expectation of the absolute difference between peak-to-peak values was calculated for each QRS complex waveform with the formula as follows:

$$E(X) = \frac{1}{N} \sum X, \quad X = |V_{\max} - V_{\min}|, \quad (3)$$

where N represents the total number of QRS complex waveforms, V_{\max} and V_{\min} denote the R and S peak value, respectively.

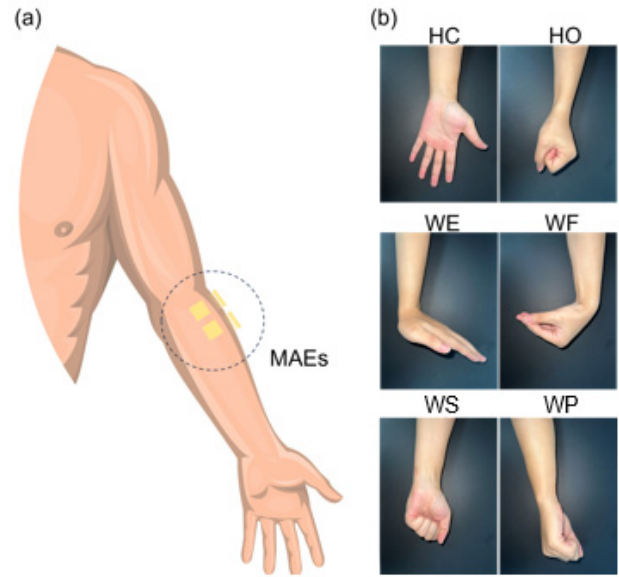


Fig. 3. (a) Electrode placement and (b) functional hand motions for EMG recording.

Second, the signal drift was calculated with the formula as follows:

$$D(Y) = \frac{1}{N} \left\{ \sum [Y - E(Y)]^2 \right\}, \quad Y = \frac{|V_{\max} + V_{\min}|}{2}, \quad (4)$$

where N represents the total number of QRS complex waveforms, V_{\max} and V_{\min} denote the R and S peak value, respectively.

Third, the square deviation of each data in ECG signals was computed with the formula as follows:

$$D(Z) = \frac{1}{N} \sum_{i=1}^N (x_i - \bar{x})^2, \quad (5)$$

where N represents the total number of data points in ECG signals, x_i denotes the i -th data point, and \bar{x} represents the mean of ECG signals.

III. RESULTS

A. Sample Characteristics

The material used of both microneedles and substrate is a biocompatible resin that was manufactured by integrated forming through the P μ SL 3D printing. Above the resin is a 50 nm thick Ti layer, which serve as a metal adhesion layer. On top of the Ti layer is a 100 nm thick Au layer, which functions as the conductive layer. The presence of these two layers of metallic conductive thin films, Ti and Au, ensures the good conductivity and biocompatibility of MAEs. Fig. 4(a) shows photographs of three different MAEs and a flat electrode, where 81, 36, and 9 microneedles are neatly arranged on the rectangular substrates in arrays of 9 \times 9, 6 \times 6, and 3 \times 3, respectively. Fig. 4(b) shows the SEM image of a typical MAE sample. The actual height of the fabricated microneedles is approximately 580 μ m, with an error of less than 10%. All microneedles have a tip diameter of approximately 8 μ m, which is highly beneficial for a smooth penetration into skin.

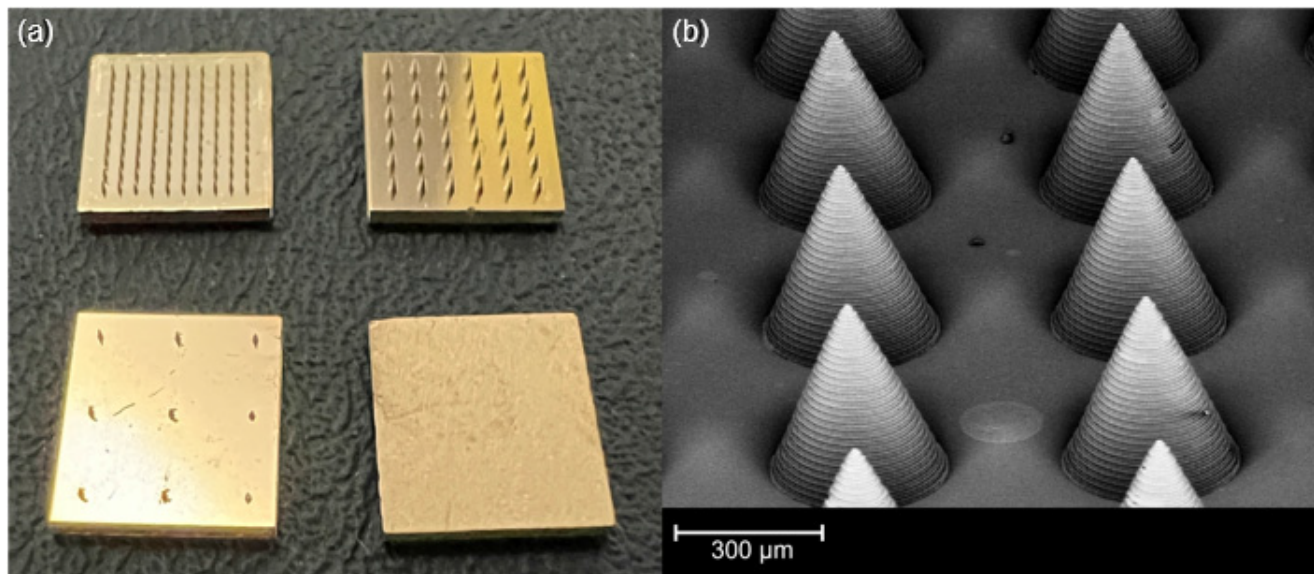


Fig. 4. (a) Photographs of MAE samples with 9×9 , 6×6 , and 3×3 microneedles on each substrate and of a flat electrode with the same dimension as MAEs. (b) The SEM image of a typical MAE sample.

B. Electrical Characteristics

Fig. 5(a) presents the curves of EII variation with frequency under the static condition for five types of electrodes. Three measurements were conducted for each type and averaged to draw the curves. The results reveal that the flat electrodes always have the highest EII, while the MAEs' EIIs are slightly greater than the gel electrodes at low frequencies and comparable at high frequencies. Notably, after the frequency exceeding 200 Hz, the EII curves of 6×6 and 9×9 MAEs virtually overlap with that of the gel electrodes. In addition, the EII of flat electrodes exhibit significant fluctuations at low-frequency stage, while the MAEs demonstrate a smooth EII performance similar to the gel electrodes. Fig. 5(b) and (c) displays the EII curves of the five types of electrodes under the pressure and dynamic conditions, respectively. Similar to Fig. 5(a), the flat electrodes have the highest impedance, followed by MAEs, and the gel electrodes own the lowest. At high frequencies, the impedance values of the MAEs and gel electrodes are comparable. These results align well with the equivalent circuit model and the aforementioned working characteristics of MAEs. It's worth noting that the EIIs of all the five types of electrodes decrease to some extent, and the flat electrodes do not show obvious fluctuations under pressure. Especially, under the dynamic condition, all the electrodes exhibit an increase of EII but very strong fluctuations are observed only on flat electrodes.

Fig. 5(d) illustrates the curves of resistance and capacitance variation with frequency ranging from 20 to 2000 Hz for the MAEs with 3×3 , 6×6 , and 9×9 microneedle arrays. The results show that at the same frequency the resistance decreases with the increase of microneedle density, while the capacitance increases. At the high-frequency stage, the resistances of the three electrodes are similar, while there are obvious differences in their capacitances.

C. EMG Acquisition

Fig. 6(a) and (b) depict the SNR of EMG signals for different hand motions recorded with MAEs, gel electrodes, and flat electrodes in the static and dynamic scenarios, respectively. In the figure, the asterisks indicate statistical significance: * denotes $p \leq 0.05$, ** denotes $p \leq 0.01$, and *** denotes $p \leq 0.001$. Generally, in the both static and dynamic scenarios, the SNR of MAEs is always greater than that of flat electrodes and comparable to that of gel electrodes. Compared with the gel electrodes, the MAEs can obtain similar SNR or even higher for some motions without significant difference, indicating a comparable EMG signal quality to that of commercial products. Compared with the flat electrodes, the MAEs show much higher SNR across all the six motions in both scenarios with statistical significances. In addition, the SNR variation of MAEs is relatively smaller than that of flat electrodes over all the motions in both scenarios, which also confirms the promising robustness of MAEs.

Fig. 7 displays the average CA over six hand motions based on the EMG acquired by using MAEs, gel electrodes, and flat electrodes. As shown in the figure, in the static scenario, there is no superiority achieved by using MAEs (96.31%), where the gel and flat electrodes can result in higher CA (98.83% and 97.16%). However, in the dynamic scenario with subjects swinging their test arms, the advantage of MAEs appears with higher CA (95.10%) and smaller variance compared with the gel and flat electrodes (93.53% and 93.01%), proving the high practicality of MAEs in clinical applications.

D. ECG Acquisition

Fig. 8(a) shows the amplitude of QRS complex of ECG recorded by using MAEs, gel electrodes, and flat electrodes. Under all the three conditions, i.e., standing still, walking on a slope, and walking on stairs, the MAEs show nearly equivalent amplitude of QRS complex as the gel electrodes, and much larger one than the flat electrodes can. Fig. 8(b) and (c) exhibit

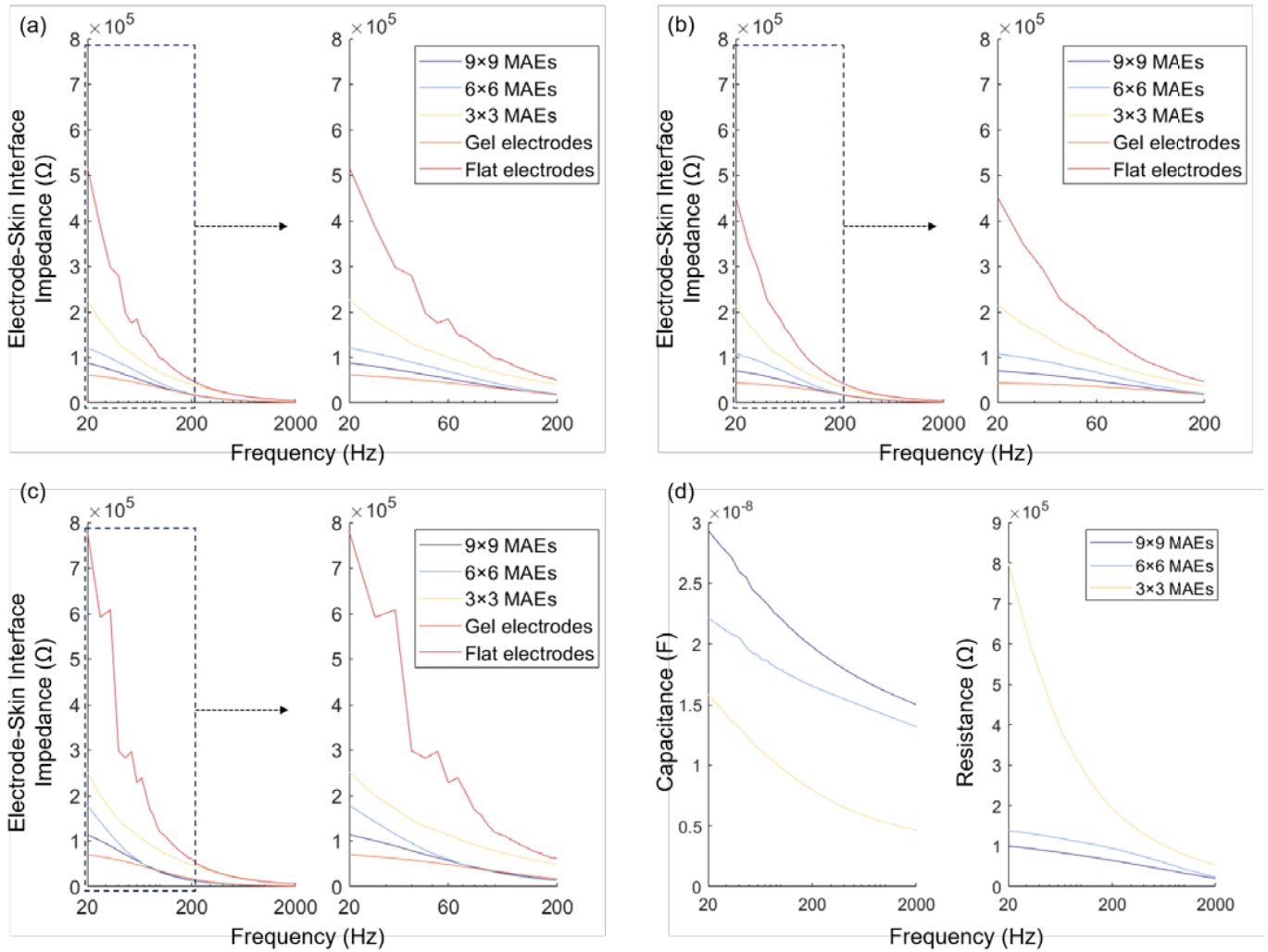


Fig. 5. The electrode-skin interface impedance (EII) for MAEs, gel electrodes, and flat electrodes in the (a) static, (b) pressure, and (c) dynamic conditions. (d) The electrode-skin interface capacitance and resistance for MAEs with 3×3 , 6×6 , and 9×9 microneedle arrays.

the signal drift and standard deviation of each data point of ECG captured by different types of electrodes. Similarly, the result of MAEs is comparable to that of the gel electrodes and lower than that of the flat electrodes. The above results as well prove the comparable performance of MAEs to commercial products in ECG recording.

IV. DISCUSSION

Electrophysiological signals hold significant importance in many fields such as disease diagnosis and rehabilitation therapy. However, these signals often possess characteristics of being weak, unstable, and challenging to capture, which imposing crucial requirements on the performances of biopotential electrodes. The concept of using MAEs for electrophysiological signal acquisition has attracted considerable attentions from researchers for several years. Nevertheless, most existing methods for MAE fabrication have shortcomings like either complex processes with high cost, or non-uniform structures with low robustness. These limitations severely hamper the large-scale production and further applications of MAEs.

In this work, we developed customizable MAEs with a distinctive three-dimensional structure. We employed a $P\mu$ SL

3D printing technology to produce the integrated electrode samples based on photosensitive resin, consisting of regular microneedle arrays erected on a substrate. The integrated structure of microneedles and substrate significantly reduces the risk of falling off of microneedles from substrates during use. The resin, as a material that can be solidified by light, can have its final mechanical property adjusted by changing the formula and photocuring parameters. The SEM image clearly demonstrates the successful structure formation through the $P\mu$ SL 3D printing technology, which greatly improves the precision of micrometric electrode fabrication compared to other 3D printing technologies. This mature and reliable technology may achieve a low-cost, fast, and stable fabrication of MAE, and it may also allow for a precise manufacture of microdevices with specific shapes and sizes. The magnetron sputtering technology was used to deposit metal conductive layers on the microneedles, where biocompatible Ti and Au layers were successively applied to ensure good adhesion and conductivity.

We studied the electrical characteristics of MAEs and compared them with the commercial products of gel electrodes and the self-made flat electrodes, which demonstrates MAEs'

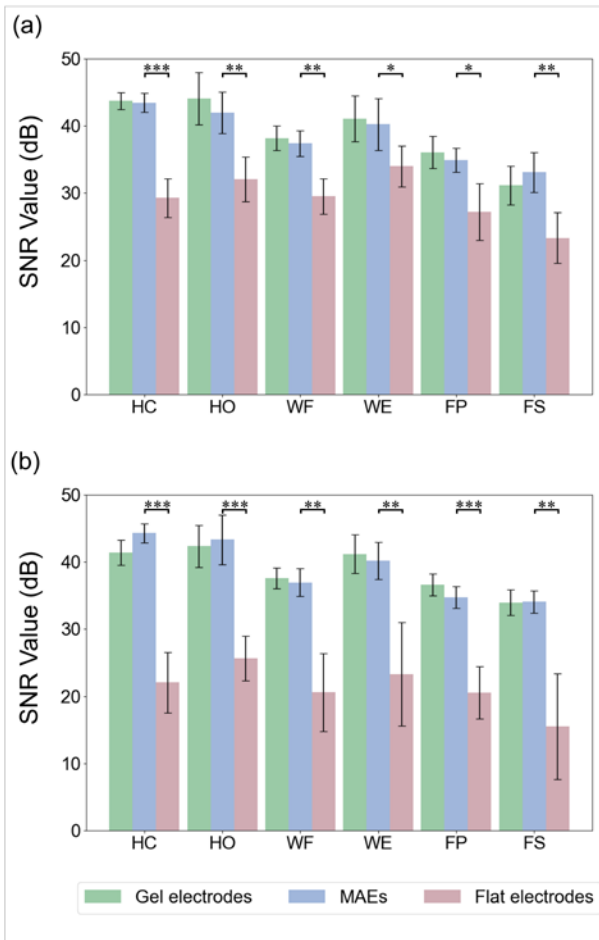


Fig. 6. The SNR of EMG signals for different hand motions recorded with MAEs, gel electrodes, and flat electrodes in the (a) static and (b) dynamic scenarios.

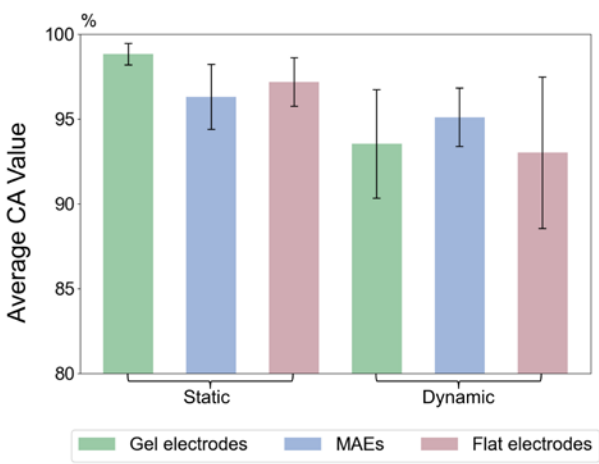


Fig. 7. The average CA over six hand motions based on the EMG acquired by using MAEs, gel electrodes, and flat electrodes in the static and dynamic scenarios.

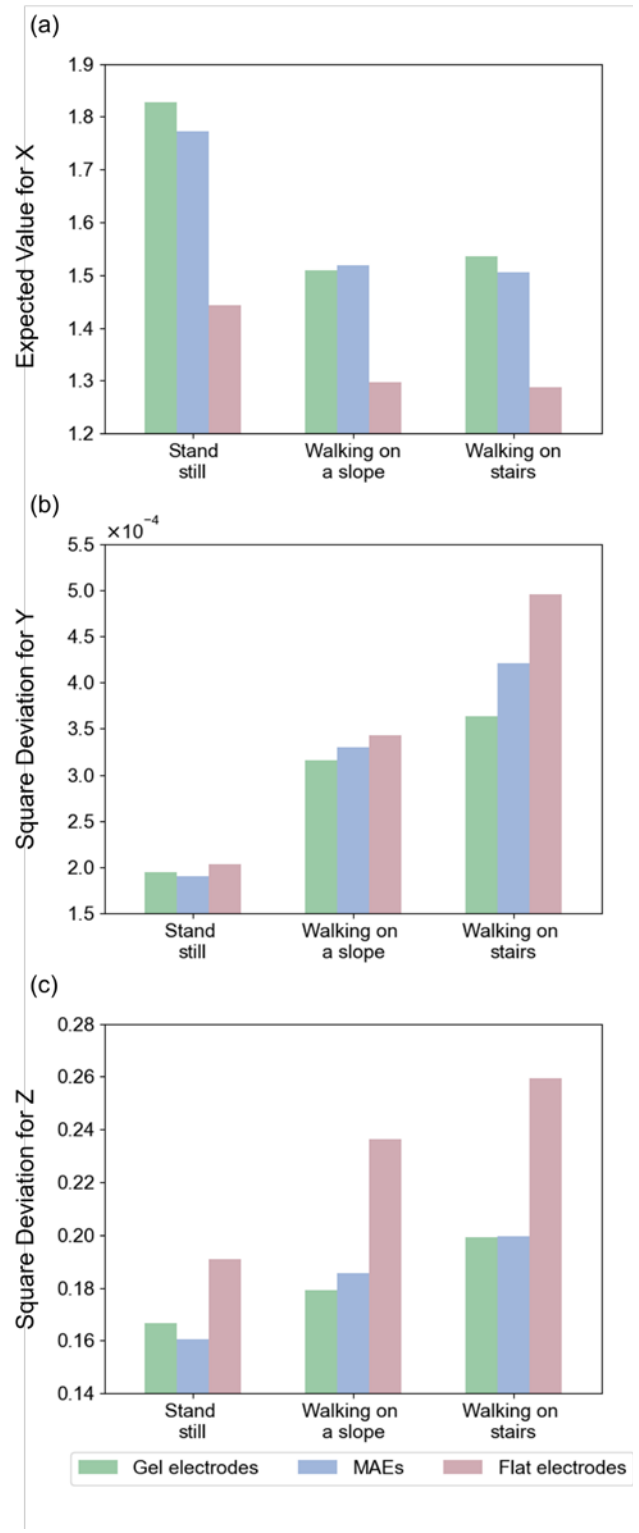


Fig. 8. The (a) amplitude of QRS complex, (b) signal drift, and (c) standard deviation of ECG recorded by using MAEs, gel electrodes, and flat electrodes in the static scenario (standing still) and dynamic scenarios (walking on a slope, and walking on stairs).

excellent EII performances. As a key factor, a lower EII may imply relatively higher signal quality and SNR, as well as smaller baseline drift. Generally, the experimental results indicate that MAEs can exhibit much lower EII in all the tested conditions compared to flat electrodes especially at low

frequencies, and show significantly less fluctuations on EII than flat electrodes and comparable to gel electrodes. These phenomena may suggest that the microneedles can effectively penetrate through the stratum corneum and establish a direct

and stable connection between the conductive viable epidermis and the outer electric circuit. Particularly, in the pressure and dynamic conditions which simply simulate the case of minor skin deformation and body movement, the EII performances of MAEs are virtually identical to gel electrodes and significantly superior to flat electrodes. This can be attributed to the stable interface between electrodes and skin fixed by the piercing of microneedles. On the other hand, as a kind of dry electrodes, the limitations of wet electrodes like dehydration of gel do not exist at all, which enables the long-term use without skin irritation. Therefore, it can be considered that MAEs may achieve performances just as good as the commercial products of gel electrodes but avoiding the shortcomings of the latter.

The EII of MAEs decreases with the increase of frequency, which may be due to the electrode-skin interface typically resembling a model of resistance and capacitance in parallel connection, serving as a barrier to block current. Moreover, there exist other resistances within the human skin tissue. As frequency continues to increase, the barrier at electrode-skin interface is breached, and the capacitance decreases with the increasing frequency. Especially in the high-frequency range, the contribution of interface capacitance to the whole impedance is much greater than that of resistance. Meanwhile, the resistance of human skin tissue does not change with frequency. Thus, as the frequency continuously increases, the EII decreases. The microneedle array density, i.e., the number of microneedles on each substrate with a fixed dimension, also influences the EII of MAEs. Across the densities of 3×3 , 6×6 , and 9×9 , it is found that the impedance value decreases with the increase of array density. This phenomenon can be explained mainly from the aspect of electrode capacitance. In a MAE, each microneedle forms a capacitor and these capacitors are all in parallel connection. Therefore, a MAE with high array density has a larger total capacitance than the one with low array density [38]. According to the equivalent circuit model, a larger capacitance implies a smaller total impedance, and thus increasing the microneedle density is beneficial for reducing the EII of MAEs. On the other hand, based on the subjective feedback from experimental operators and subjects, increasing the number of microneedles requires a stronger pressure to insert the microneedles into skin, which may cause discomfort. Thus, a balance between the microneedle number and EII performance is important for the optimization of MAEs.

For EMG recording, the results of SNR demonstrate that MAEs can obtain high-quality signals, which is as good as gel electrodes and significantly superior to flat electrodes. This observation aligns with the EII testing, further confirming the enhanced stability and anti-interference capability of MAEs. In terms of CA, although MAEs do not exhibit better results than gel and flat electrodes in the static scenario (standing still), however, in the dynamic scenario (standing with arm swinging), MAEs can achieve the highest average CA. Additionally, the average variation of CA by MAEs in both static and dynamic scenarios is the smallest, proving the stable signal acquisition by MAEs. It is noteworthy that the CA can be influenced by the robustness of EMG pattern-recognition algorithm, and subsequent studies might probe

further into specific algorithms especially suitable for MAEs. For ECG recording, the results show that it is able to capture clear P-waves, T-waves, and QRS complex from the ECG signals by using all the tested electrodes in the static scenario (standing still). While in the dynamic scenarios (walking on a slope and stairs) the ECG signals collected by MAEs and gel electrodes display a high degree of similarity in all the scenarios, showing larger peak-to-peak amplitude, reduced signal drift, and smaller data point square deviation compared to flat electrodes. This highlights the superior performance of the metal-viable epidermal interface formed by the microneedles piercing into skin especially during body motions, both in terms of signal strength and stability. Overall, from the experimental results of EII, EMG recording, and ECG recording it can be concluded that MAEs can effectively mitigate the influence of high-impedance stratum corneum and establish a stable interface with skin, which significantly enhance the electrophysiological signal quality.

With the well-designed structure and stable conductivity, the MAEs prepared in this work allow for signal recording in an ultra-minimally invasive or non-invasive manner. Considering the biocompatible properties of the materials used for MAE fabrication, i.e., the biocompatible resin and Ti and Au layers, together with the IRB-approved research protocol, the safety of experiments was firstly ensued. Following the application of MAEs, only micrometer-scale depressions were left caused by the microneedles' penetration, which typically disappeared completely within approximately ten to twenty minutes without any treatment. No skin allergy, inflammation, injury, or any other side effect was reported by all subjects after experiments. This phenomenon indicates that the microneedles did not touch the dermal layer to harm subjects' nerves. The MAEs samples fabricated in this work have a height of approximately $580 \mu\text{m}$ while the thickness of human epidermal layer is around $220 \mu\text{m}$. Thus, it is inferred that maximally $\sim 1/3$ of the needle length can penetrate into skin, while the remaining part is outside. Coincidentally, the uniform spaces between microneedles outside skin create multiple ventilation channels when a MAE attached to skin, which may help to alleviate the accumulation of sweat during application, which enhances the wearing comfort of MAEs compared with that of other electrodes.

Based on the findings of this research, it is recommended that future studies may try more electrophysiological signals such as electroencephalograms (EEG). However, due to the large difference between the scalp and muscle surface, e.g., the interference from dense hairs, sensitive and easy-to-get-injured characters of scalp, and different thickness of scalp, the structure design, material processing, and packaging technique of MAEs for EEG recording on scalp would be quite different those for EMG and ECG recording on muscle surface. Besides, it should expand participant sample size and design various clinical scenarios to further study the characteristics of MAEs. Moreover, except for electrophysiological recording, the use of MAEs for electrical stimulation might be another topic worth to explore. In general, the unique attributes of MAEs present considerable research and we can anticipate more innovative applications of MAEs.

V. CONCLUSION

This work presented an easy-to-perform method for fabricating MAEs by using the P μ SL 3D printing technology. The well-designed three-dimensional structure of MAEs offers outstanding performances in EII and subsequently high-quality electrophysiological acquisition through an ultra-minimally invasive or non-invasive approach without hurting human skin. Various applications of MAEs in human-machine interfaces and human-machine interactions are highly anticipated.

REFERENCES

- [1] Y. M. Chi, T. P. Jung, and G. Cauwenberghs, "Dry-contact and non-contact biopotential electrodes: Methodological review," *IEEE Rev. Biomed. Eng.*, vol. 3, pp. 106–119, 2010.
- [2] Y. Wang et al., "Electrically compensated, tattoo-like electrodes for epidermal electrophysiology at scale," *Sci. Adv.*, vol. 6, no. 43, Oct. 2020, Art. no. eabd0996.
- [3] E. Farago, D. MacIsaac, M. Suk, and A. D. C. Chan, "A review of techniques for surface electromyography signal quality analysis," *IEEE Rev. Biomed. Eng.*, vol. 16, pp. 472–486, 2023.
- [4] T. Kim, J. Vanloo, and W. S. Kim, "3D origami sensing robots for cooperative healthcare monitoring," *Adv. Mater. Technol.*, vol. 6, no. 3, Mar. 2021, Art. no. 2000938.
- [5] H. Kim, R. F. Yazicioglu, P. Merken, C. Van Hoof, and H.-J. Yoo, "ECG signal compression and classification algorithm with quad level vector for ECG Holter system," *IEEE Trans. Inf. Technol. Biomed.*, vol. 14, no. 1, pp. 93–100, Jan. 2010.
- [6] S. Patel, H. Park, P. Bonato, L. Chan, and M. Rodgers, "A review of wearable sensors and systems with application in rehabilitation," *J. NeuroEng. Rehabil.*, vol. 9, no. 1, p. 21, Dec. 2012.
- [7] R. Li, C. Zhao, C. Wang, J. Wang, and Y. Zhang, "Enhancing fNIRS analysis using EEG rhythmic signatures: An EEG-informed fNIRS analysis study," *IEEE Trans. Biomed. Eng.*, vol. 67, no. 10, pp. 2789–2797, Oct. 2020.
- [8] A. Saha, A. Konar, A. Chatterjee, A. Ralescu, and A. K. Nagar, "EEG analysis for olfactory perceptual-ability measurement using a recurrent neural classifier," *IEEE Trans. Human-Mach. Syst.*, vol. 44, no. 6, pp. 717–730, Dec. 2014.
- [9] L. Tian et al., "Large-area MRI-compatible epidermal electronic interfaces for prosthetic control and cognitive monitoring," *Nature Biomed. Eng.*, vol. 3, no. 3, pp. 194–205, Feb. 2019.
- [10] L. Wang, J. Liu, B. Yang, and C. Yang, "PDMS-based low cost flexible dry electrode for long-term EEG measurement," *IEEE Sensors J.*, vol. 12, no. 9, pp. 2898–2904, Sep. 2012.
- [11] P. Griss, P. Enoksson, H. Tolvanen-Laakso, P. Merilainen, S. Ollmar, and G. Stemme, "Spiked biopotential electrodes," in *Proc. IEEE 13th Annu. Int. Conf. Micro Electro Mech. Syst.*, Jan. 2000, pp. 323–328.
- [12] T. Kato, A. Ueno, S. Kataoka, H. Hoshino, and Y. Ishiyama, "An application of capacitive electrode for detecting electrocardiogram of neonates and infants," in *Proc. Int. Conf. IEEE Eng. Med. Biol. Soc.*, Aug. 2006, pp. 916–919.
- [13] A. K. Srivastava, B. Bhartia, K. Mukhopadhyay, and A. Sharma, "Long term biopotential recording by body conformable photolithography fabricated low cost polymeric microneedle arrays," *Sens. Actuators A, Phys.*, vol. 236, pp. 164–172, Dec. 2015.
- [14] J.-Y. Baek, J.-H. An, J.-M. Choi, K.-S. Park, and S.-H. Lee, "Flexible polymeric dry electrodes for the long-term monitoring of ECG," *Sens. Actuators A, Phys.*, vol. 143, no. 2, pp. 423–429, May 2008.
- [15] Y. Fu, J. Zhao, Y. Dong, and X. Wang, "Dry electrodes for human bioelectrical signal monitoring," *Sensors*, vol. 20, no. 13, p. 3651, Jun. 2020.
- [16] P. Leleux et al., "Ionic liquid gel-assisted electrodes for long-term cutaneous recordings," *Adv. Healthcare Mater.*, vol. 3, no. 9, pp. 1377–1380, Sep. 2014.
- [17] C.-T. Lin, L.-D. Liao, Y.-H. Liu, I.-J. Wang, B.-S. Lin, and J.-Y. Chang, "Novel dry polymer foam electrodes for long-term EEG measurement," *IEEE Trans. Biomed. Eng.*, vol. 58, no. 5, pp. 1200–1207, May 2011.
- [18] F. Stauffer et al., "Skin conformal polymer electrodes for clinical ECG and EEG recordings," *Adv. Healthcare Mater.*, vol. 7, no. 7, Apr. 2018, Art. no. 1700994.
- [19] G.-L. Li, J.-T. Wu, Y.-H. Xia, Q.-G. He, and H.-G. Jin, "Review of semi-dry electrodes for EEG recording," *J. Neural Eng.*, vol. 17, no. 5, Oct. 2020, Art. no. 051004.
- [20] G. Li, S. Wang, M. Li, and Y. Y. Duan, "Towards real-life EEG applications: Novel superporous hydrogel-based semi-dry EEG electrodes enabling automatically 'charge-discharge' electrolyte," *J. Neural Eng.*, vol. 18, no. 4, Aug. 2021, Art. no. 046016.
- [21] G. Li et al., "Polyvinyl alcohol/polyacrylamide double-network hydrogel-based semi-dry electrodes for robust electroencephalography recording at hairy scalp for noninvasive brain-computer interfaces," *J. Neural Eng.*, vol. 20, no. 2, Apr. 2023, Art. no. 026017.
- [22] J. M. Benítez and F. J. Montáns, "The mechanical behavior of skin: Structures and models for the finite element analysis," *Comput. Struct.*, vol. 190, pp. 75–107, Oct. 2017.
- [23] F. Lu et al., "Review of stratum corneum impedance measurement in non-invasive penetration application," *Biosensors*, vol. 8, no. 2, p. 31, Mar. 2018.
- [24] M. F. Leyva-Mendivil, A. Page, N. W. Bressloff, and G. Limbert, "A mechanistic insight into the mechanical role of the stratum corneum during stretching and compression of the skin," *J. Mech. Behav. Biomed. Mater.*, vol. 49, pp. 197–219, Sep. 2015.
- [25] E. Forvi et al., "Preliminary technological assessment of microneedles-based dry electrodes for biopotential monitoring in clinical examinations," *Sens. Actuators A, Phys.*, vol. 180, pp. 177–186, Jun. 2012.
- [26] W. Zhou et al., "Fabrication and impedance measurement of novel metal dry bioelectrode," *Sens. Actuators A, Phys.*, vol. 201, pp. 127–133, Oct. 2013.
- [27] G. S. Guvanasen et al., "A stretchable microneedle electrode array for stimulating and measuring intramuscular electromyographic activity," *IEEE Trans. Neural Syst. Rehabil. Eng.*, vol. 25, no. 9, pp. 1440–1452, Sep. 2017.
- [28] S. Indermun et al., "Current advances in the fabrication of microneedles for transdermal delivery," *J. Controlled Release*, vol. 185, pp. 130–138, Jul. 2014.
- [29] Y. Wang et al., "Towards improving the quality of electrophysiological signal recordings by using microneedle electrode arrays," *IEEE Trans. Biomed. Eng.*, vol. 68, no. 11, pp. 3327–3335, Nov. 2021.
- [30] L.-S. Hsu, S.-W. Tung, C.-H. Kuo, and Y.-J. Yang, "Developing barbed microtip-based electrode arrays for biopotential measurement," *Sensors*, vol. 14, no. 7, pp. 12370–12386, Jul. 2014.
- [31] T. Fofonoff et al., "Mechanical assembly of a microelectrode array for use in a wireless intracortical recording device," in *Proc. 2nd Annu. Int. IEEE-EMBS Special Topic Conf. Microtechnolog. Med. Biol.*, Oct. 2002, pp. 269–272.
- [32] K. Chen, L. Ren, Z. Chen, C. Pan, W. Zhou, and L. Jiang, "Fabrication of micro-needle electrodes for bio-signal recording by a magnetization-induced self-assembly method," *Sensors*, vol. 16, no. 9, p. 1533, Sep. 2016.
- [33] C. Pan et al., "Magnetization-induced self-assembly method: Micro-needle array fabrication," *J. Mater. Process. Technol.*, vol. 227, pp. 251–258, Jan. 2016.
- [34] L. Ren et al., "Flexible microneedle array electrode using magnetorheological drawing lithography for bio-signal monitoring," *Sens. Actuators A, Phys.*, vol. 268, pp. 38–45, Dec. 2017.
- [35] K. J. Krieger, N. Bertollo, M. Dangol, J. T. Sheridan, M. M. Lowery, and E. D. O'Ceirbhail, "Simple and customizable method for fabrication of high-aspect ratio microneedle molds using low-cost 3D printing," *Microsystems Nanoeng.*, vol. 5, no. 1, Sep. 2019, Art. no. 42.
- [36] G. Li, S. Wang, and Y. Y. Duan, "Towards conductive-gel-free electrodes: Understanding the wet electrode, semi-dry electrode and dry electrode-skin interface impedance using electrochemical impedance spectroscopy fitting," *Sens. Actuators B, Chem.*, vol. 277, pp. 250–260, Dec. 2018.
- [37] L. Ren, B. Liu, W. Zhou, and L. Jiang, "A mini review of microneedle array electrode for bio-signal recording: A review," *IEEE Sensors J.*, vol. 20, no. 2, pp. 577–590, Jan. 2020.
- [38] R. Soltanzadeh, E. Afsharipour, C. Shafai, N. Anssari, B. Mansouri, and Z. Moussavi, "Molybdenum coated SU-8 microneedle electrodes for transcutaneous electrical nerve stimulation," *Biomed. Microdevices*, vol. 20, no. 1, p. 1, Nov. 2017.